Title

Influence of the Location and Zone of Tumor in Prostate Cancer Detection and Localization on 3-T Multiparametric MRI Based on PI-RADS Version 2.

Journal

American Journal of Roentgenology, 214(5)

Authors

Wibulpolprasert, Pornphan
Raman, Steven
Hsu, William
et al.

Publication Date

2020-05-01

DOI

10.2214/AJR.19.21608

Peer reviewed

HHS Public Access

Author manuscript

AJR Am J Roentgenol. Author manuscript; available in PMC 2024 July 30.

Published in final edited form as:

AJR Am J Roentgenol. 2020 May ; 214(5): 1101–1111. doi:10.2214/AJR.19.21608.

Influence of the Location and Zone of Tumor in Prostate Cancer Detection and Localization on 3-T Multiparametric MRI Based on PI-RADS Version 2

Pornphan Wibulpolprasert[1], **Steven S. Raman**[2,3], **William Hsu**[2], **Daniel J. A. Margolis**[2], **Nazanin H. Asvadi**[2], **Pooria Khoshnoodi**[2], **Amin Moshksar**[2], **Nelly Tan**[2], **Preeti Ahuja**[2], **Cleo K. Maehara**[2], **Anthony Sisk**[4], **James Sayre**[2], **David S. K. Lu**[2], **Robert E. Reiter**[3]

[1]Department of Diagnostic and Therapeutic Radiology, Faculty of Medicine, Ramathibodi Hospital, 270 Rama VI Rd, Bangkok 10400, Thailand.

[2]Department Radiology, David Geffen School of Medicine at UCLA, Los Angeles, CA.

[3]Department of Urology, David Geffen School of Medicine at UCLA, Los Angeles, CA.

[4]Department of Pathology and Laboratory Medicine, David Geffen School of Medicine at UCLA, Los Angeles, CA.

Abstract

OBJECTIVE.—The objective of our study was to determine the performance of 3-T multiparametric MRI (mpMRI) for prostate cancer (PCa) detection and localization, stratified by anatomic zone and level, using Prostate Imaging Reporting and Data System version 2 (PI-RADSv2) and whole-mount histopathology (WMHP) as reference.

MATERIALS AND METHODS.—Multiparametric MRI examinations of 415 consecutive men were compared with thin-section WMHP results. A genitourinary radiologist and pathologist collectively determined concordance. Two radiologists assigned PI-RADSv2 scores and sector location to all detected foci by consensus. Tumor detection rates were calculated for clinical and pathologic (tumor location and zone) variables. Both rigid and adjusted sector-matching models were used to account for fixation-related issues.

RESULTS.—Of 863 PCa foci in 16,185 prostate sectors, the detection of overall and index PCa lesions in the midgland, base, and apex was 54.9% and 83.1%, 42.1% and 64.0% ($p = 0.04$, $p = 0.02$), and 41.9% and 71.4% ($p = 0.001$, $p = 0.006$), respectively. Tumor localization sensitivity was highest in the midgland compared with the base and apex using an adjusted match compared with a rigid match (index lesions, 71.3% vs 43.7%; all lesions, 70.8% vs 36.0%) and was greater in the peripheral zone (PZ) than in the transition zone. Three-Tesla mpMRI had similarly high specificity (range, 93.8–98.3%) for overall and index tumor localization when using both rigid and adjusted sector-matching approaches.

CONCLUSION.—For 3-T mpMRI, the highest sensitivity (83.1%) for detection of index PCa lesions was in the midgland, with 98.3% specificity. Multiparametric MRI performance for

Address correspondence to P. Wibulpolprasert (punlee77@gmail.com).

sectoral localization of PCa within the prostate was moderate and was best for index lesions in the PZ using an adjusted model.

Keywords

prostate cancer; prostate sector map; tumor location; tumor zone

The ability to detect and localize prostate cancer (PCa) with high spatial fidelity is one of the main goals of any noninvasive PCa imaging techniques in the era of targeted biopsy and focal therapy. Three-Tesla multiparametric MRI (mpMRI) is considered the best non-invasive imaging modality for detection, characterization, grading, staging, targeted biopsy guidance, focal treatment planning, and posttreatment surveillance for PCa [1–3]. According to various characteristics of PCa in different zones and the diversity of prostate biopsy techniques, different performances of mpMRI stratified by prostate anatomic zone [4, 5] and location of tumor [6–8] have been reported. Many methods have been proposed for localization of PCa on 3-T mpMRI compared with the reference standard whole-mount histopathology (WMHP) results, including the updated Prostate Imaging Reporting and Data System version 2 (PI-RADSv2), which was published in 2015 [9]. PI-RADSv2 is designed to provide a global standardized lexicon for interpretation of mpMRI and localization of PCa using a 39-segmentation map of the prostate. However, a contemporary, detailed, large-scale analysis of the performance of 3-T mpMRI for PCa detection and localization stratified by level (base, midgland, apex) and zone (peripheral zone [PZ] and transition zone [TZ]) with a reference standard of thin-section WMHP results using the 39-segmentation prostate model has not been performed to our knowledge.

The study group and method of prostate model matching between mpMRI and WMHP results for this study were also used in another study that reported the overall and sector-based performance of mpMRI [10]; however, the data analysis and study objective for this study differ from those of [10]. The purpose of this study was to determine the performance of 3-T mpMRI for PCa detection and localization, stratified by anatomic zone and level, using PI-RADSv2 and WMHP as reference.

Materials and Methods

Patients

This retrospective study complied with 1996 HIPAA and was approved by the institutional review board with a waiver of informed consent. The study group for this single-institution observational study was composed of 415 consecutive men who underwent 3-T mpMRI of the prostate gland before robotic-assisted radical prostatectomy (RALP) between December 2009 and August 2016. The mean patient age was 61.1 years (age range, 38.0–80.0 years), and the mean prostate-specific antigen (PSA) level was 8.1 ng/mL (median, 6.0 ng/mL; range, 12.0–155.0 ng/mL). Patients underwent mpMRI at least 6 weeks after transrectal ultrasound (TRUS)-guided biopsy to minimize biopsy-related hemorrhage effects and within 90–120 days of radical prostatectomy.

MRI Technique

All patients underwent prostate MRI on one of several 3-T scanners (Magnetom Trio, Skyra, or Verio; all, Siemens Healthineers) using similar protocols and with endorectal and pelvic external phased-array coils. The endorectal coil (tuned to 127.8 MHz; BPX-15, Medrad) was inserted using a semianesthetic gel (benzocaine gel, Hurricaine, Beutlich Pharmaceuticals) or nonanesthetic lubricant (Surgilube, Savage Laboratories) while the patient was in the left lateral decubitus position. The balloon surrounding the coil was distended with 50 mL of perfluorocarbon (3 mmol/L; Fluorinert, 3M) to reduce susceptibility artifacts induced by air in the balloon of the coil. An antiperistaltic agent (1 mg of glucagon; GlucaGen, Lilly) was administered intramuscularly to reduce bowel peristalsis.

The imaging protocol included triplanar T2-weighted turbo spin-echo (TSE) MRI, DWI, axial unenhanced T1-weighted MRI, and axial 3D fast-field echo dynamic contrast-enhanced MRI (DCE-MRI) sequences. A small-FOV 3D axial TSE T2-weighted sequence was performed using spatial-encoded and chemical-shift–encoded excitation (SPACE [sampling perfection with application optimized contrast using different flip angle evolutions], Siemens Healthineers) and the following parameters: TR range/TE, 3800–5040/101; echo-train length, 13; FOV, 14 cm; matrix, 256 × 256; and 1.5-mm contiguous slices. For the DWI sequence, echo-planar imaging was used with the following parameters: TR/TE, 3900/60; FOV, 21 × 26 cm; matrix, 130 × 160; slice thickness and gap, 3.6 and 0 mm; and number of signals acquired, 4. The b values were 0, 100, and 800 s/mm^2 with a calculated or natively acquired b value of 1400 s/mm^2. A dynamic view-sharing time-resolved angiography with stochastic trajectories gradientecho T1-weighted sequence was performed over 6 minutes (4.75 seconds per acquisition) with a 15-second injection delay (TWIST [time-resolved angiography with interleaved stochastic trajectories], Siemens Healthineers). The following parameters were used: TR/TE, 3.9/1.4; flip angle, 12°; FOV, 26 × 26 cm; matrix, 160 × 160; and slice thickness and gap, 3.6 and 0 mm. Axial DCE-MR images were obtained before, during, and after a single-dose injection of gadopentetate dimeglumine (Magnevist, Bayer) at a dose of 0.1 mg/kg through a peripheral vein at a rate of 2 mL/s. The study was then transferred to a separate workstation (DynaCAD, InVivo) for processing of the DW images and DCE-MR images for interpretation.

Imaging Analysis

Each 3-T mpMRI study was interpreted by an abdominal imaging fellow (postgraduate year 6, reviewer 1) and one of three board-certified genitourinary abdominal imaging subspecialized radiologists with 22, 18, and 10 years of experience in interpreting prostate MRI (reviewers 2, 3, and 4, respectively). Each abdominal imaging radiologist interpreted the study using T2-weighted images, T1-weighted images, high-b-value (b = 1400 s/mm^2) DW images, apparent diffusion coefficient (ADC) maps, and DCE-MR images. Individual lesions were identified and localized within the prostate. The radiologists performed assessments using a 5-point scale based on PI-RADSv2, which combines mpMRI findings on T2-weighted imaging, DWI, and DCE-MRI correlates with the likelihood of the presence of clinically significant PCa. By definition, a category 1 lesion indicated a very low suspicion for clinically significant PCa, whereas a category 5 lesion was very highly suspicious for clinically significant PCa. All suspicious lesions were manually mapped to

the 39-segmentation PI-RADSv2 prostate model by two radiologists (reviewers 3 and 7) with 18 and 8 years of experience in prostate MRI. The primary sector assigned to each lesion was defined as the center of the lesion. PZ lesions were assigned to a sector using DWI as the primary sequence and TSE T2-weighted imaging as the secondary sequence, and TZ lesions were assigned to a sector using TSE T2-weighted imaging as the primary sequence and DWI as the secondary sequence.

Whole-Mount Histopathology Analysis

Thin-section WMHP preparations of the RALP-derived prostatectomy specimens were performed by dedicated genitourinary pathology technologists and supervised by a dedicated, experienced genitourinary pathologist (reviewer 8, with 6 years of experience in prostate pathology). The fresh whole prostate specimen was placed inside a patient-specific 3D-printed mold of 91 patients of our population. The prostatectomy specimen was inked at its apical and basal sides and was fixed in buffered neutral formalin for 24–28 hours at room temperature after removal of the seminal vesicles and apical segments. The prostate gland was section entirely in the axial plane in 5-mm increments from the base to the apex perpendicular to the urethral plane to approximate an axial MR image. Each slice was photographed on both the basal and apical sides and fixed for another 24 hours and then underwent whole-mount paraffin embedding. Individual whole-mount sections from each slice were obtained at 5 μm for histopathologic H and E staining and were mounted on a large glass slide for WMHP analysis.

On each WMHP section, the genitourinary pathologist identified and outlined each individual PCa lesion and recorded its largest diameter; location; primary and secondary Gleason patterns; and its relationship to the capsule, veins, and nerves. The index lesion was defined as the PCa focus with the highest Gleason grade. In cases of multifocal lesions, the index PCa lesion was defined as the lesion with the highest Gleason grade or the largest lesion. A satellite PCa lesion was defined as a nonindex lesion (i.e., multifocal lesions that had lower grade or were smaller than the index lesion). Clinically significant PCa was defined as any lesion greater than 0.5 cm^3 with a Gleason score (GS) or 7 or greater or a Gleason 6 lesion that was larger than 1.5 cm. Pathologic TNM staging was also reported. The seminal vesicles and apical sections were similarly evaluated after whole-mount fixation.

Correlation of Imaging Data With Histopathologic Findings

On a monthly basis, a joint radiology-pathology matching meeting was held by a genitourinary radiologist (reviewer 3) and genitourinary pathologist (reviewer 8) to rereview 3-T mpMRI in the context of the finalized WMHP findings. Each PCa lesion detected and graded on WMHP was matched to possible foci on 3-T mpMRI. All lesions were assigned a sextant-based location within the prostate and also assigned a sextant and location (right vs left, anterior vs posterior). The location and zone of each lesion were determined by the center of the lesion. True-positive (TP) lesions matched in location on WMHP and 3-T mpMRI; false-positive (FP) were lesions that were seen only on 3-T mpMRI. Lesions detected only on WMHP but not on 3-T mpMRI were categorized as false-negative (FN).

During a separate session, two genitourinary radiologists (reviewers 3 and 7) in consensus manually mapped each 3-T mpMRI focus and WMHP lesion as well as primary sector (center) of each lesion into the 39-segmentation PI-RADSv2 prostate model for per-sector analysis. This segmentation model from the PI-RADSv2 sector map uses 39 sectors (i.e., regions): 36 for the prostate gland (12 sectors for base, mid, and apical levels, equally), two for the seminal vesicles, and one for the external urethral sphincter [9]. Each whole-mount slide was scanned at high resolution (300-dpi scanner) and also digitally photographed at a magnification of 10× and 100× and archived electronically in our database. The segmental prostate model used for mapping was similar to those used for imaging evaluation to allow radiologic findings-pathologic findings correlation.

Correlation of MR images with WMHP sections in this study was based in part on techniques reported in a previous study [11] that was performed before PI-RADSv2 was published. In that study [11], the authors tried to account for difficulties in radiologic-pathologic correlation due to lack of in situ anatomic connective tissue. There was variable loss of prostate volume from fixation and processing depending on the proportion of fibrous tissue to muscle in each gland. We matched each suspicious focus on 3-T mpMRI with each detected lesion on WMHP to minimize errors from potential gland deformation, fixation-related shrinkage, and inherent variability in slice orientation and thickness. Two approaches were used to map each TP and FN lesion by sector using PI-RADSv2. The first approach, the rigid sector-matching approach, is a more stringent approach that did not make any adjustment for fixation-related issues and required that all suspicious foci on mpMRI match exactly on a sector-by-sector basis with each lesion on WMHP for a positive match (TP). The second approach, the adjusted sector-matching approach, is a less stringent approach for a TP match for which all suspicious foci on mpMRI need only to approximately match segments and predefined adjacent segments were allowed to account for misalignment between pathologic sections and the mpMR images. Contiguous or immediate adjacent sectors in the same axial plane as well as one contiguous adjacent pathologically defined primary sector on 39-segmentation PI-RADSv2 prostate model when radiologic findings and pathologic findings were compared. For example, each of the 39 sectors had six to 10 predefined adjacent sectors that were considered adjusted matches between WMHP lesions and mpMRI foci (Fig. 1). The adjusted sector approach aims to ameliorate the effect of minor mismatches between WMHP and mpMRI and allow determination of accuracy within a certain distance without observer bias from either the radiologist or pathologist.

Each suspicious focus on mpMRI was classified as a FP if it failed to meet the specific rigid or adjusted match criteria. Lesions identified only on WMHP (i.e., lacking an mpMRI correlate) were classified as FNs for both rigid and adjusted analyses. For index lesion analysis, only sectors with designated index lesions on WMHP were included as TP and sectors with satellite lesions (nonindex PCa lesions [i.e., multifocal lesions that had lower grade or were smaller than the index lesion]) were excluded.

Statistical Analysis

Correlation between mpMRI findings and WMHP findings was performed by a per-lesion analysis and a per-sector analysis. For the per-sector analysis, we separately evaluated the

results using the rigid and adjusted sector match approaches. The sensitivity of mpMRI was defined as the probability of correctly identifying a WMHP-proven positive PCa sector in either rigid or adjusted analysis. Specificity was defined as the rigid and adjusted match between mpMRI and WMHP segments without PCa. This strategy ensures the probability of test results that are negative for tumor at a particular region, given that the particular region (rigid sector-matching approach) and all contiguous adjusted sectors (adjusted sector-matching approach) are negative for tumor at pathologic analysis.

The chi-square analysis was performed for categoric variables, and the Student *t* test was performed for continuous variables. All statistical analyses was performed using Stata software (version 13.0, StataCorp) and SAS software (version 9.3, SAS Institute). Statistical significance was defined as $p < 0.05$.

Results

Per-Lesion Analysis

The study cohort included 415 patients with 863 PCa lesions detected, outlined, graded, and staged on WMHP by reviewers who were blinded to mpMRI results. Of 415 patients, 159 (38.3%) had a solitary PCa lesion, whereas 256 (61.7%) had from two to seven tumor foci. Overall, 414 of 863 PCa lesions (47.9%) were detected on 3-T mpMRI. Of 863 PCa foci, 441 (51.1%), 346 (40.1%), and 76 (8.8%) were in the midgland, apex, and base, respectively. Overall, 643 PCa lesions (74.5%) and 220 (25.5%) were located in the PZ and TZ. Most patients had pT2 PCa (276 patients [66.5%]), and the remaining patients had pT3 lesions (pT3a, 109 [26.3%]; pT3b, 30 [7.2%]). The mean diameters of PCa lesions overall by location were 1.6 cm (range, 0.05–5.0 cm) in the midgland, 1.3 cm (range, 0.1–4.2 cm) in the apex, and 1.2 cm (range, 0.1–3.5 cm) in the base.

Of 415 index lesions, 236 (56.9%), 154 (37.1%), and 25 (6.0%) were in the midgland, apex, and base, respectively. Of the 415 index lesions, 311 (74.9%) and 104 (25.1%) were located in the PZ and TZ. Mean diameters of index PCa lesions at midgland, apex, and base were 2.2 cm (range, 0.2–5.0 cm), 2.0 cm (range, 0.15–4.2 cm), and 2.1 cm (range, 0.5–3.5 cm) (Table 1).

For midgland lesions, 3-T mpMRI detected 242 of 441 (54.9%) lesions and 196 of 236 (83.1%) index lesions. There were significantly more midgland lesions than both apical lesions (all lesions, 145/346 [41.9%], $p = 0.001$; index lesions, 110/154 [71.4%], $p = 0.006$) and basal lesions (all lesions, 32/76 [42.1%], $p = 0.04$; index lesions, 16/25 [64.0%], $p = 0.02$). The lesion detection rate was slightly but nonsignificantly higher for PZ lesions than for TZ lesions (all lesions, 324/643 [50.4%] vs 95/220 [43.2%], $p = 0.22$; index lesions, 246/311 [79.1%] vs 76/104 [73.1%], $p = 0.20$). There was no significant difference in rate of detection of all basal and apical PCa lesions and index basal and apical PCa lesions (Table 2 and Fig. 2).

Per-Sector Analysis

A total of 16,185 individual prostate sectors were analyzed in 415 patients (39 per patient). For tumor location, 4980 sectors (12 per patient) was analyzed for base, midgland, and

apical levels, equally. For zonal anatomy, overall 8300 sectors (20 per patient) was analyzed for PZ and 6640 sectors (16 per patient) for TZ. Overall, 830 sectors (2 per patient) were also analyzed for seminal vesicle tumor involvement.

On WMHP, PCa was identified in 3559 of 16,185 sectors (22.0%), and 2513 sectors had index PCa lesions. For the 3559 positive tumor sectors, 1531 (43.0%) were midgland tumor sectors, 1430 (40.2%) were apical sectors, 562 (15.8%) were basal sectors, and 36 (1.0%) were seminal vesicle sectors.

The mpMRI sensitivity of tumor localization for both overall and index PCa lesions was significantly greater for adjusted sector-matching approach than for the rigid sector-matching approach. The sensitivity of overall and index PCa localization in the midgland (rigid, 36.0% vs 43.7%; adjusted, 70.8% vs 71.3%) was significantly greater than in the apex (rigid, 23.0% vs 29.0%; adjusted, 49.1% vs 47.8% [$p < 0.05$]) or base (rigid, 19.0% vs 21.0%; adjusted, 35.8% vs 34.0% [$p < 0.05$]), respectively. The sensitivity of PCa localization was significantly greater in the PZ than the TZ for both overall PCa (rigid, 30.3% vs 24.5% [$p < 0.001$]; adjusted, 58.9% vs 51.2% [$p = 0.04$]) and index PCa (rigid, 37.0% vs 29.2% [$p < 0.001$]; 58.4% vs 50.5% [$p = 0.001$]), respectively. Both adjusted and rigid sector-matching approaches showed similar high specificity for overall and index tumor localization (93.8–98.3%, Tables 3 and 4).

The sensitivity and specificity for overall tumor localization in the seminal vesicle sectors by mpMRI were 55.6% (20/36) and 99.8% (792/794), respectively. The most frequently detected TP tumor sector (108/415, 26.0%) by mpMRI was sector 23, which was right posterior PZ of the mid prostate level. The two most frequently identified true-negative (TN) tumor sectors were the right (398/415, 95.9%) and left (394/415, 94.9%) seminal vesicles. The most frequent FP and FN sectors were right posterior basal PZ (sector 11, 37/415 [8.9%]) and right anterior PZ at mid prostate level (sector 21, 129/415 [31.1%]), respectively (Fig. 3).

Figure 4 illustrates a good match between 3-T mpMRI with WMHP findings in a midgland PCa lesion in a 49-year-old man with high serum PSA level. Figure 5 illustrates a nontarget lesion at segment 21, which is the most frequent FN sector in our study, that was missed on mpMRI.

Discussion

Three-Tesla mpMRI is currently regarded as the most sensitive and specific imaging technique for the preoperative evaluation of organ-confined PCa, including detection, staging, and localization and for the preoperative prediction of tumor aggressiveness [12]. Several recent studies have reported a wide range of incidence and accuracy values of PCa tumor detection by mpMRI, as well as oncologic outcomes between PCa in different locations [6, 8, 13]. To our knowledge, no studies have reported tumor localization using the PI-RADSv2 sector-based mapping template.

In this study, we found that overall and index PCa lesions were frequently localized in the mid prostate gland followed by apex and base in order of decreasing frequency. The rate

of tumor detection was the best for index PCa lesions in the midgland (83.1%) compared with index PCa lesions in the apex and base. These results are partially consistent with those reported by Tan et al. [8] in a cohort of 122 patients, with WMHP findings as the reference standard, that showed mpMRI had significantly higher overall detection rates at the midgland or base than at the apex. Wefer et al. [6] also reported the best performance of mpMRI in midgland sextants compared with apex or base in a cohort of 47 patients and 250 sextants.

Because of a number of potential factors (i.e., the complex histology of apical prostate gland, less demarcated capsule, poorly confined glandular elements, and possibly absent surrounding periprostatic fat), the detection, localization, and resection of apical PCa lesions have been challenging on imaging and biopsy where PCa is undersampled [8, 14, 15]. Another reason for not detecting many lesions in the apex and base is that the tissue composition is clearly different between the apex (primarily stroma with low ADC values and hypointense signal on T2-weighted imaging), midgland and base (mostly densely glandular tissue in the central zone that can mimic PCa) as shown by Langer et al. [16] and Chatterjee et al. [17]. At the prostatic base, the periphery of the prostate gland is composed predominantly of prostatic stroma, which merges imperceptibly with the bladder musculature and the stroma of the seminal vesicles, possibly increasing risk of seminal vesicle invasion. Lee et al. [18] showed a significant association between seminal vesicle invasion and biochemical recurrence in cases of base-dominant PCa. Relative to the base and apex, the histology of the midgland is less complex, partially enabling relatively better mpMRI performance for PCa. Furthermore, the presence of a positive margin in a radical prostatectomy specimen was a significant risk factor for a worse prognosis, especially at apical and posterolateral margins, which were common locations [19–23]. Therefore, precise definition of extent and location of PCa is one of the most important role of preoperative mpMRI for treatment planning that may influence treatment outcome and long-term prognosis.

To our knowledge, this investigation is among the largest to date for evaluation of 3-T mpMRI performance for tumor localization based on zones and the 39-segmentation PI-RADSv2 scheme. Because we mapped both TP and FP lesions and TN and FN lesions, we were able to estimate not only sensitivity but also the sector-based specificity and accuracy of 3-T mpMRI for PCa detection in the largest reported cohort to date. The TN rate was estimated on the basis of the fraction of 39 sectors lacking PCa in each of 415 thin-section WMHP specimens and for a total of 16,185 prostate sectors over the entire cohort. Furthermore, we applied two alternative analytic approaches—a rigid match and an adjusted sector match—for correlation between suspicious lesions from mpMRI with WMHP sections.

When compared with rigid localization, the adjusted localization had higher overall sensitivity for all lesions and index lesions, especially in midgland index tumors (71.3%) compared with index lesions at the apex and base, and had high specificities, which were similar in different locations, for all lesions and index lesions (94.0–98.0%). Our results validate three earlier pilot studies that did not use PI-RADSv2: Turkbey et al. [11], Rosenkrantz et al. [24], and Isebaert et al. [25].

In a study by Turkbey et al. [11] with a cohort of 70 patients (30 segments per prostate), mpMRI was performed at 3 T with an endorectal coil using a combination of T2-weighted imaging, DCE-MRI, and MR spectroscopy without DWI; Turkbey et al. reported the highest sensitivity for tumor detection was 72% and 43% for adjusted and rigid approaches, respectively, and that tumor localization was best for PCa lesions with a GS of 7 or greater and PCa lesions larger than 3 mm. Rosenkrantz et al. [24] used an inferior stepsection histopathology technique as a reference standard in a cohort of 51 patients (18 segments per prostate) on a 3-T scanner without an endorectal coil. They found improvement of sensitivity for tumor localization of 75.9% for the adjusted method compared with 60.2% for the rigid method and greater sensitivity for index lesions with a GS of 6 or greater and index lesions 1 cm or larger.

In a cohort of 75 patients (24 segments per prostate) who underwent 1.5-T mpMRI using T2-weighted imaging, DWI, and DCE-MRI without an endorectal coil, Isebaert et al. [25] reported sensitivity and specificity of 49.3% and 86.5%, respectively, by a stringent (rigid) approach and 58.5% sensitivity and 84.3% specificity by a clinical (adjusted) approach for overall PCa localization.

The overall lower sensitivity and higher specificity for PCa localization in our results is probably because of the greater number of prostate sectors designated in PI RADSv2. In addition, we also chose to delineate only the most suspicious foci from combined mpMRI pulse sequences. We believe they represent the most accurate localization ability of 3-T mpMRI. Although high in specificity for PCa localization, low sensitivity suggests that mpMRI should be carefully interpreted along with biopsy results for local therapy planning to completely delineate the true extent of lesions. Furthermore, in the recently published study on prostate sector model, Greer et al. [26] showed poor reproducibility when attempting to define tumor location within the PI-RADSv2 map. The PI-RADSv2 map presents a challenge because it compresses 15–25 cross-sectional axial mpMR images into three planes. These data suggest that the PI-RADSv2 map should be used very cautiously for actual biopsy guidance even though it may be adequate for indicating the general area of PCa.

Using PI-RADSv2, we found that the sensitivity of overall PZ and TZ tumor detection was similar for both overall (50.4% vs 43.2%) and index lesions (79.1% vs 73.1%). For tumor localization, sensitivity of mpMRI in the PZ was significantly greater than in the TZ for overall lesions (rigid model, 30.3% vs 24.5%; adjusted model, 58.9% vs 51.2%) and for index lesions (rigid model, 37.0% vs 29.2%; adjusted model, 58.4% vs 50.5%). Our results are similar to prior pilot studies [4, 5, 27] that showed overall similar or better sensitivities for tumor detection in the PZ relative to the TZ. These results are partially secondary to basic histologic and functional difference between the two zones [14] as well as heterogeneous signal intensity with coexisting benign prostate hyperplasia that can mimic or mask the appearance of TZ tumors. In the updated PI-RADSv2 [9, 28], evaluation of PZ lesions relies primarily on DW images and ADC maps and evaluation of TZ lesions relies primarily on T2-weighted images to improve MRI performance and minimize overlap with benign prostatic hyperplastic nodules.

Our study had limitations that must be acknowledged. First, the cohort is subject to selection bias inherent within a surgical population required for WMHP comparison, and the results may not be broadly applicable to nonsurgical populations. Second, we did not exclude nontarget lesions detected on mpMRI, especially any hemorrhagic segments, from the analysis because these findings are a routine component of daily clinical practice and influence MRI interpretation. Third, the intra- and interobserver variabilities were not measured in our study. Finally, there is potential for incorrect estimation using the adjusted sector match approach if sensitivity depends on the number of TP sectors in a given patient.

Despite these limitations, to date, this study is the largest study to evaluate the performance of 3-T mpMRI with WMHP correlation stratified by location (base, midgland, apex) and zone (PZ and TZ) of tumor. In this sector-based analysis, we were able to calculate specificity by MRI-negative sectors and the TN sectors in all men who had malignancy confirmed by WMHP results. We found that mpMRI has greater sensitivity for PCa detection and localization for midgland tumors than tumors in the apex or base and that mpMRI has greater sensitivity for PZ tumors than TZ tumors. Using 3-T mpMRI and the PI-RADSv2 in the largest reported cohort to date, we found that mpMRI achieved the highest sensitivity (83.1%) for detection of index lesions at the midgland with 98.3% specificity.

Acknowledgments

We thank Rathachai Kaewlai for editorial assistance and Voraparee Suvannarerg and Sohrab Afshari Mirak for figure editing.

Supported in part by the Department of Radiology and Pathology Integrated Diagnostics (IDx) Program and Specialized Program of Research Excellence (SPORE) of Prostate Cancer.

References

1. Murphy G, Haider M, Ghai S, Sreeharsha B. The expanding role of MRI in prostate cancer. AJR 2013; 201:1229–1238 [PubMed: 24261361]
2. Le JD, Tan N, Shkolyar E, et al. Multifocality and prostate cancer detection by multiparametric magnetic resonance imaging: correlation with whole-mount histopathology. Eur Urol 2015; 67:569–576 [PubMed: 25257029]
3. Hoeks CM, Barentsz JO, Hambrock T, et al. Prostate cancer: multiparametric MR imaging for detection, localization, and staging. Radiology 2011; 261:46–66 [PubMed: 21931141]
4. Asvadi NH, Afshari Mirak S, Mohammadian Bajgiran A, et al. 3T multiparametric MR imaging, PIRADSv2-based detection of index prostate cancer lesions in the transition zone and the peripheral zone using whole mount histopathology as reference standard. Abdom Radiol (NY) 2018; 43:3117–3124 [PubMed: 29725743]
5. Russo F, Regge D, Armando E, et al. Detection of prostate cancer index lesions with multiparametric magnetic resonance imaging (mpMRI) using whole-mount histological sections as the reference standard. BJU Int 2016; 118:84–94 [PubMed: 26198404]
6. Wefer AE, Hricak H, Vigneron DB, et al. Sextant localization of prostate cancer: comparison of sextant biopsy, magnetic resonance imaging and magnetic resonance spectroscopic imaging with step section histology. J Urol 2000; 164:400–404 [PubMed: 10893595]
7. Schouten MG, van der Leest M, Pokorny M, et al. Why and where do we miss significant prostate cancer with multi-parametric magnetic resonance imaging followed by magnetic resonance-guided and transrectal ultrasound-guided biopsy in biopsy-naïve men? Eur Urol 2017; 71:896–903 [PubMed: 28063613]

8. Tan N, Margolis DJ, Lu DY, et al. Characteristics of detected and missed prostate cancer foci on 3-T multiparametric MRI using an endorectal coil correlated with whole-mount thin-section histopathology. AJR 2015; 205:[web]W87–W92 [PubMed: 26102423]
9. Weinreb JC, Barentsz JO, Choyke PL, et al. PI-RADS Prostate Imaging - Reporting and Data System: 2015, Version 2. Eur Urol 2016; 69:16–40 [PubMed: 26427566]
10. Wibulpolprasert P, Raman SS, Hsu W, et al. Detection and localization of prostate cancer at 3-T multiparametric MRI using PI-RADS segmentation. AJR 2019; 212:[web]W122–W131 [PubMed: 30995090]
11. Turkbey B, Pinto PA, Mani H, et al. Prostate cancer: value of multiparametric MR imaging at 3-T for detection—histopathologic correlation. Radiology 2010; 255:89–99 [PubMed: 20308447]
12. Ueno Y, Tamada T, Bist V, et al. Multiparametric magnetic resonance imaging: current role in prostate cancer management. Int J Urol 2016; 23:550–557 [PubMed: 27184019]
13. Kim M, Choi SK, Park M, et al. Characteristics of anteriorly located prostate cancer and the usefulness of multiparametric magnetic resonance imaging for diagnosis. J Urol 2016; 196:367–373 [PubMed: 26997311]
14. Coakley FV, Hricak H. Radiologic anatomy of the prostate gland: a clinical approach. Radiol Clin North Am 2000; 38:15–30 [PubMed: 10664664]
15. Ohori M, Abbas F, Wheeler TM, Kattan MW, Scardino PT, Lerner SP. Pathological features and prognostic significance of prostate cancer in the apical section determined by whole mount histology. J Urol 1999; 161:500–504 [PubMed: 9915435]
16. Langer DL, van der Kwast TH, Evans AJ, et al. Prostate tissue composition and MR measurements: investigating the relationships between ADC, T2, K(trans), v(e), and corresponding histologic features. Radiology 2010; 255:485–494 [PubMed: 20413761]
17. Chatterjee A, Watson G, Myint E, Sved P, McEntee M, Bourne R. Changes in epithelium, stroma, and lumen space correlate more strongly with Gleason pattern and are stronger predictors of prostate ADC changes than cellularity metrics. Radiology 2015; 277:751–762 [PubMed: 26110669]
18. Lee YI, Lee HM, Jo JK, et al. . Association between seminal vesicle invasion and prostate cancer detection location after transrectal systemic biopsy among men who underwent radical prostatectomy. PloS One 2016; 11:e0148690
19. Watson RB, Civantos F, Soloway MS. Positive sur-gical margins with radical prostatectomy: detailed pathological analysis and prognosis. U rology 1996; 48:80–90
20. Öbek C, Sadek S, Lai S, Civantos F, Rubinowicz D, Soloway MS. Positive surgical margins with radical retropubic prostatectomy: anatomic site-specific pathologic analysis and impact on prognosis. Urology 1999; 54:682–688 [PubMed: 10510928]
21. van den Ouden D, Bentvelsen FM, Boevé ER, Schröder FH. Positive margins after radical prostatectomy: correlation with local recurrence and distant progression. Br J Urol 1993; 72:489–494 [PubMed: 7505193]
22. EasthAm JA, Kuroiwa K, Ohori M, et al. Prognostic significance of location of positive margins in radical prostatectomy specimens. Urology 2007; 70:965–969 [PubMed: 18068455]
23. Blute ML, Bostwick DG, Bergstralh EJ, et al. Anatomic site-specific positive margins in organ-confined prostate cancer and its impact on outcome after radical prostatectomy. Urology 1997; 50:733–739 [PubMed: 9372884]
24. Rosenkrantz AB, Deng FM, Kim S, et al. Prostate cancer: multiparametric MRI for index lesion localization—a multiple-reader study. AJR 2012; 199:830–837 [PubMed: 22997375]
25. Isebaert S, Van den Bergh L, Haustermans K, et al. Multiparametric MRI for prostate cancer localization in correlation to whole-mount histopathology. J Magn Reson Imaging 2013; 37:1392–1401 [PubMed: 23172614]
26. Greer MD, Shih JH, Barrett T, et al. All over the map: an interobserver agreement study of tumor location based on the PI-RADSv2 sector map. J Magn Reson Imaging 2018; 48:482–490 [PubMed: 29341356]
27. Rosenkrantz AB, Kim S, Lim RP, et al. Prostate cancer localization using multiparametric MR imaging: comparison of Prostate Imaging Reporting and Data System (PI-RADS) and Likert scales. Radiology 2013; 269:482–492 [PubMed: 23788719]

28. Barentsz JO, Weinreb JC, Verma S, et al. Synopsis of the PI-RADS v2 guidelines for multiparametric prostate magnetic resonance imaging and recommendations for use. Eur Urol 2016; 69:41–49 [PubMed: 26361169]

29. American College of Radiology. PI-RADS: Prostate Imaging–Reporting and Data System 2015, version 2. Reston, VA: American College of Radiology, 2015

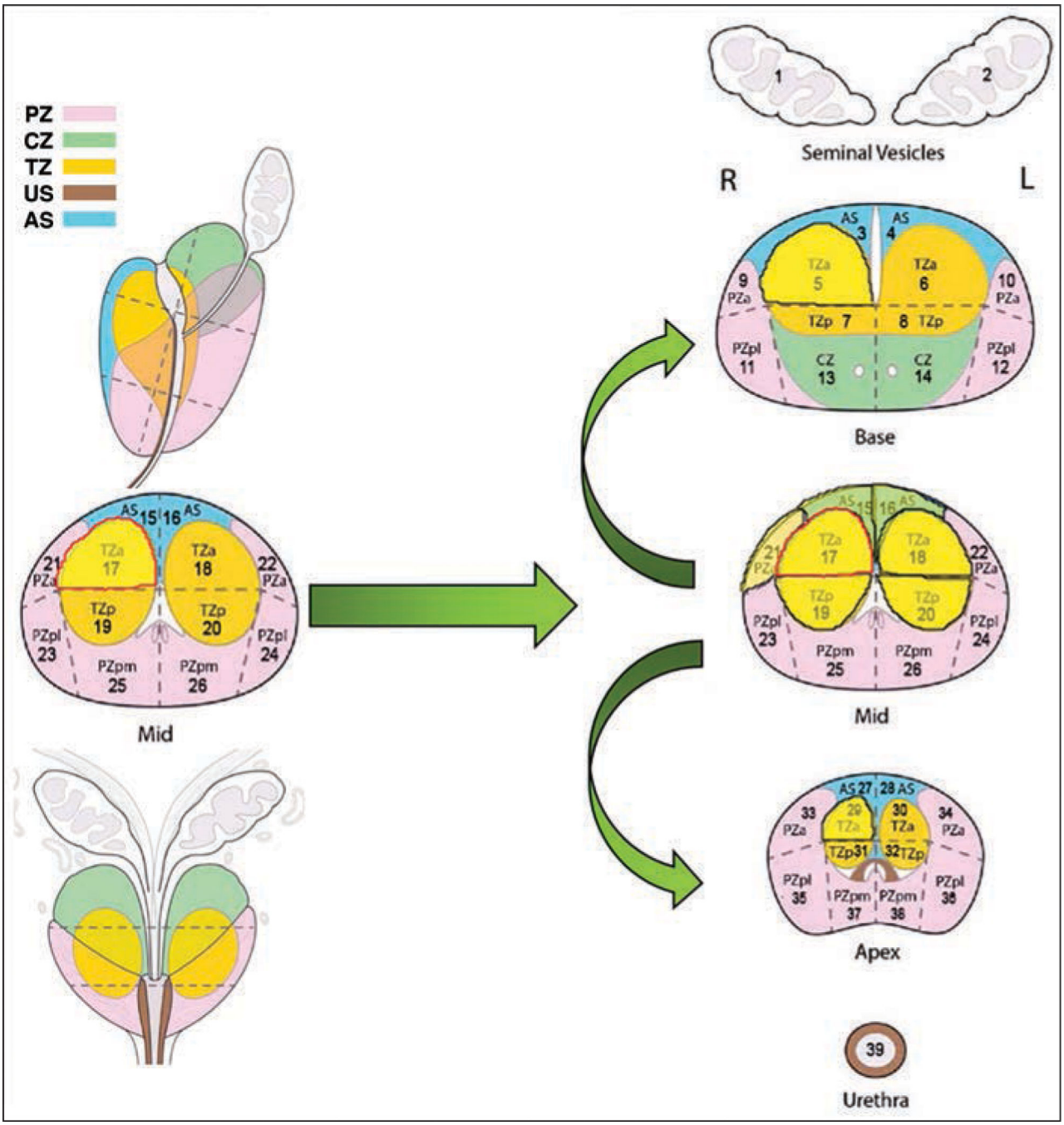

Fig. 1—.

Illustration shows adjusted sector-matching approach used for multiparametric MRI and whole-mount histopathology correlation based on 39-segmentation prostate model from Prostate Imaging Reporting and Data System version 2. Numbers refer to sector number. In this example, adjusted sector match of sector 17 at right (R) anterior TZ (*outlined areas*) is shown. Sectors 15, 16, 18, 19, 20, and 21 were defined as true-positive (TP) contiguous adjacent sectors in same plane, and sectors 5 and 29 were defined as TP sectors in upper and lower directions (*arrows*). PZ = peripheral zone, CZ = central zone, TZ = transition zone,

US = urethral sphincter, AS = anterior fibromuscular stroma, a = anterior, p = posterior, pl = posterolateral, pm = posteromedial, L = left. (Adapted from American College of Radiology, PI-RADS: Prostate Imaging–Reporting and Data System 2015, version 2. Reston, VA: American College of Radiology, 2015 [29], with permission from the American College of Radiology)

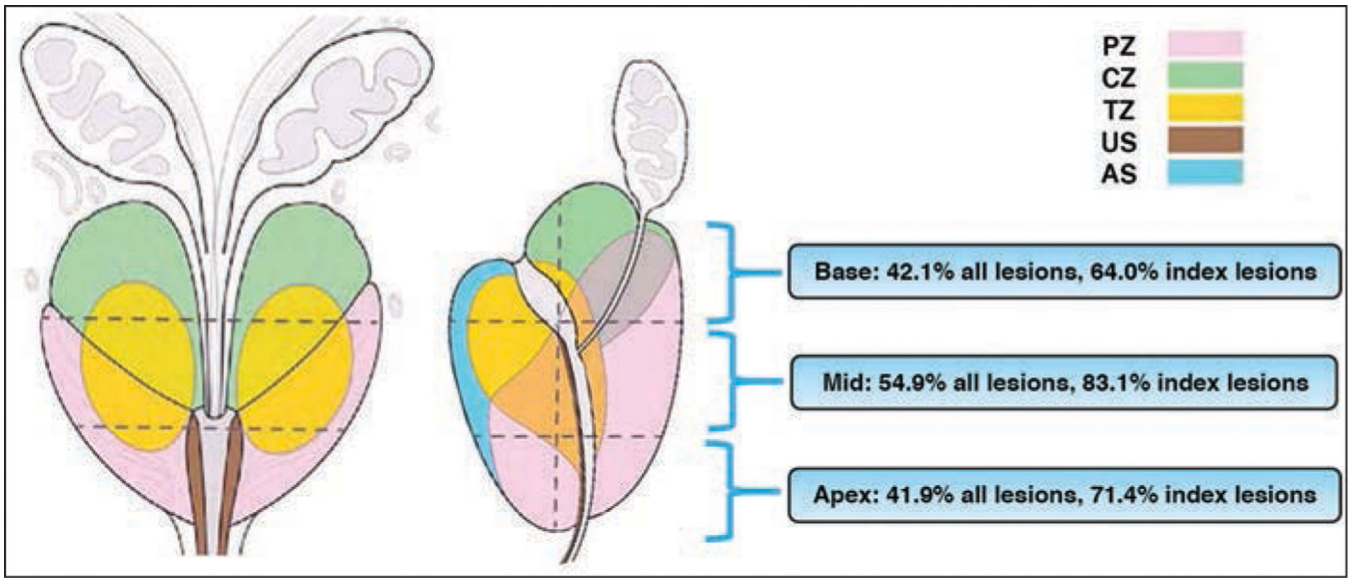

Fig. 2—.

Distribution map shows prostate cancer detection rates of multiparametric MRI for overall tumors and index tumors stratified by anatomic prostate level: base, midgland, and apex. PZ = peripheral zone, CZ = central zone, TZ = transition zone, US = urethral sphincter, AS = anterior fibromuscular stroma. (Adapted from American College of Radiology, PI-RADS: Prostate Imaging–Reporting and Data System 2015, version 2. Reston, VA: American College of Radiology, 2015 [29], with permission from the American College of Radiology)

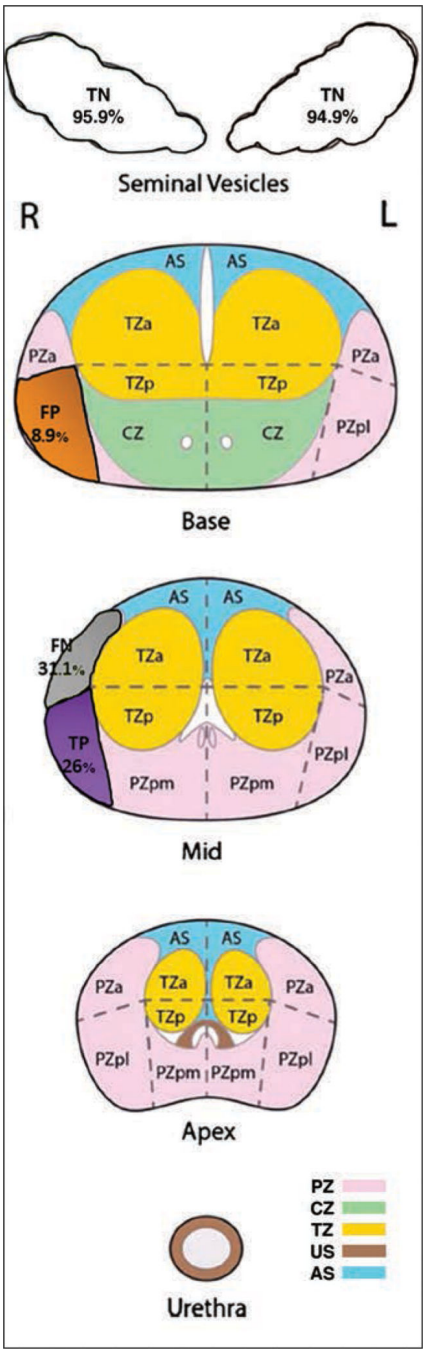

Fig. 3—.

Distribution maps of most frequently detected true-positive (TP, *purple*) tumor sectors, true-negative (TN, *white*) tumor sectors, and false-positive (FP, *orange*), and false-negative (FN, *gray*) sectors on multiparametric MRI. PZ = peripheral zone, CZ = central zone, TZ = transition zone, US = urethral sphincter, AS = anterior fibromuscular stroma, a = anterior, p = posterior, pl = posterolateral, pm = posteromedial. (Adapted from American College of Radiology, PI-RADS: Prostate Imaging–Reporting and Data System 2015, version 2.

Reston, VA: American College of Radiology, 2015 [29], with permission from the American College of Radiology)

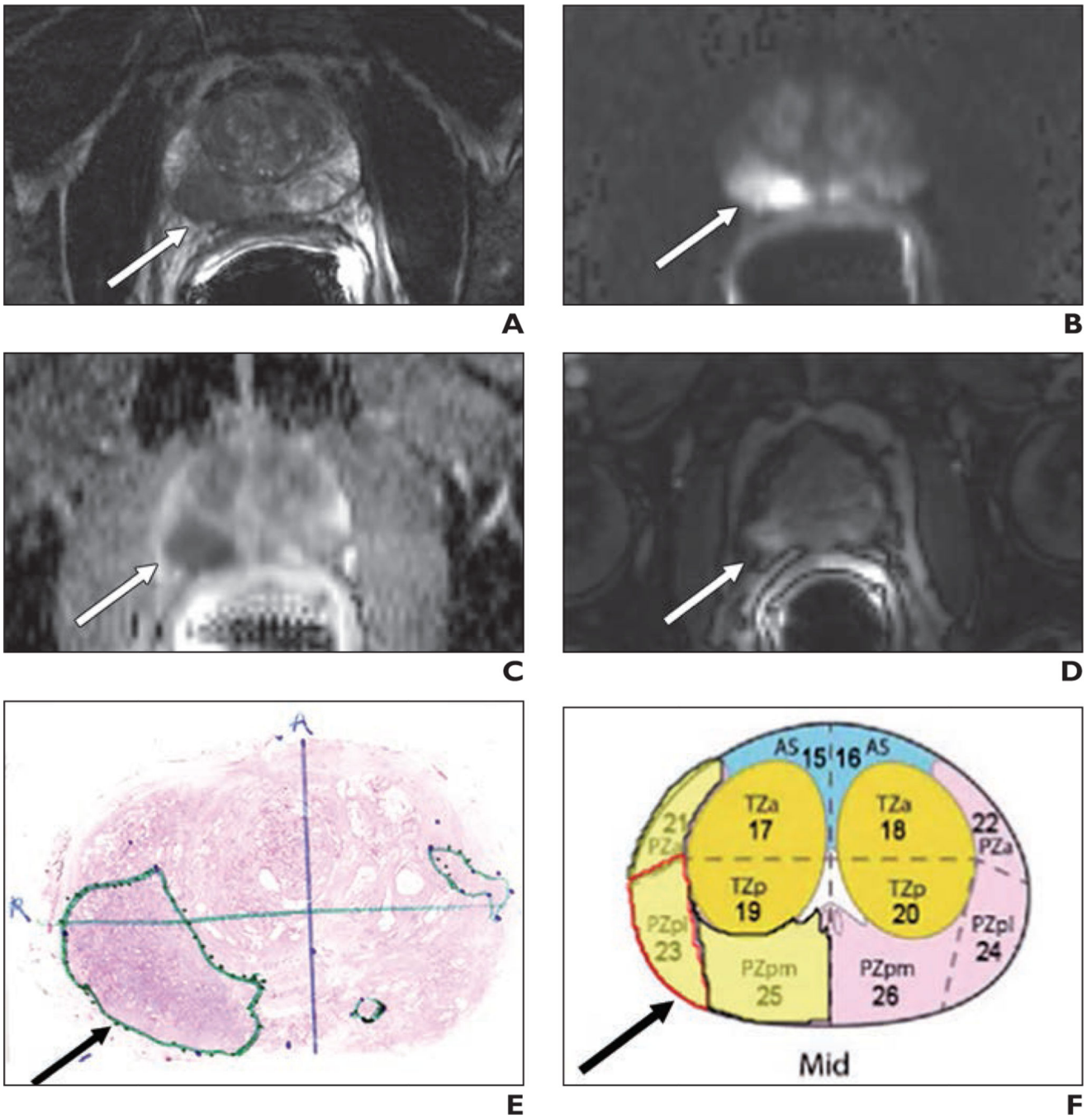

Fig. 4—.

Example case of good match between multiparametric MRI (mpMRI) findings and whole-mount histopathology (WMHP) results is shown. Patient is 49-year-old man who was referred for prostate mpMRI because of high serum prostate-specific antigen value (9.3 ng/mL).

A, Axial T2-weighted image shows 2.0-cm hypointense lesion in right posterior peripheral zone with right extracapsular invasion (*arrow*).

B and **C,** DW image (**B**) and apparent diffusion coefficient map (**C**) show marked restricted diffusion (*arrow*) in area corresponding to hypointense lesion on T2-weighted image (**A**).
D, Dynamic contrast-enhanced MR image shows focal early enhancement (*arrow*) in area corresponding to hypointense lesion on T2-weighted image (**A**).
E, Photomicrograph of thin section from whole-mount preparation of specimen obtained at radical prostatectomy shows 2.9-cm tumor (*arrow* and *large outlined area*; Gleason score 4 + 4) in right (R) posterior midlevel of prostate gland with right extracapsular extension. Small outlined areas show another foci of non target prostate cancer lesions.
A = anterior.
F, Drawing of prostate sector map based on Prostate Imaging Reporting and Data System version 2 (PI-RADSv2). Numbers refer to sector number. WMHP results (**E**) show primary sector is right posterior midgland (sector 23, *arrow* and *red outline*). Overall assessment was category 5 according to PI-RADSv2. AS = anterior fibromuscular stroma, PZ = peripheral zone, TZ = transition zone, a = anterior, p = posterior, pl = posterolateral, pm = posteromedial. (Adapted from American College of Radiology, PI-RADS: Prostate Imaging–Reporting and Data System 2015, version 2. Reston, VA: American College of Radiology, 2015 [29], with permission from the American College of Radiology)

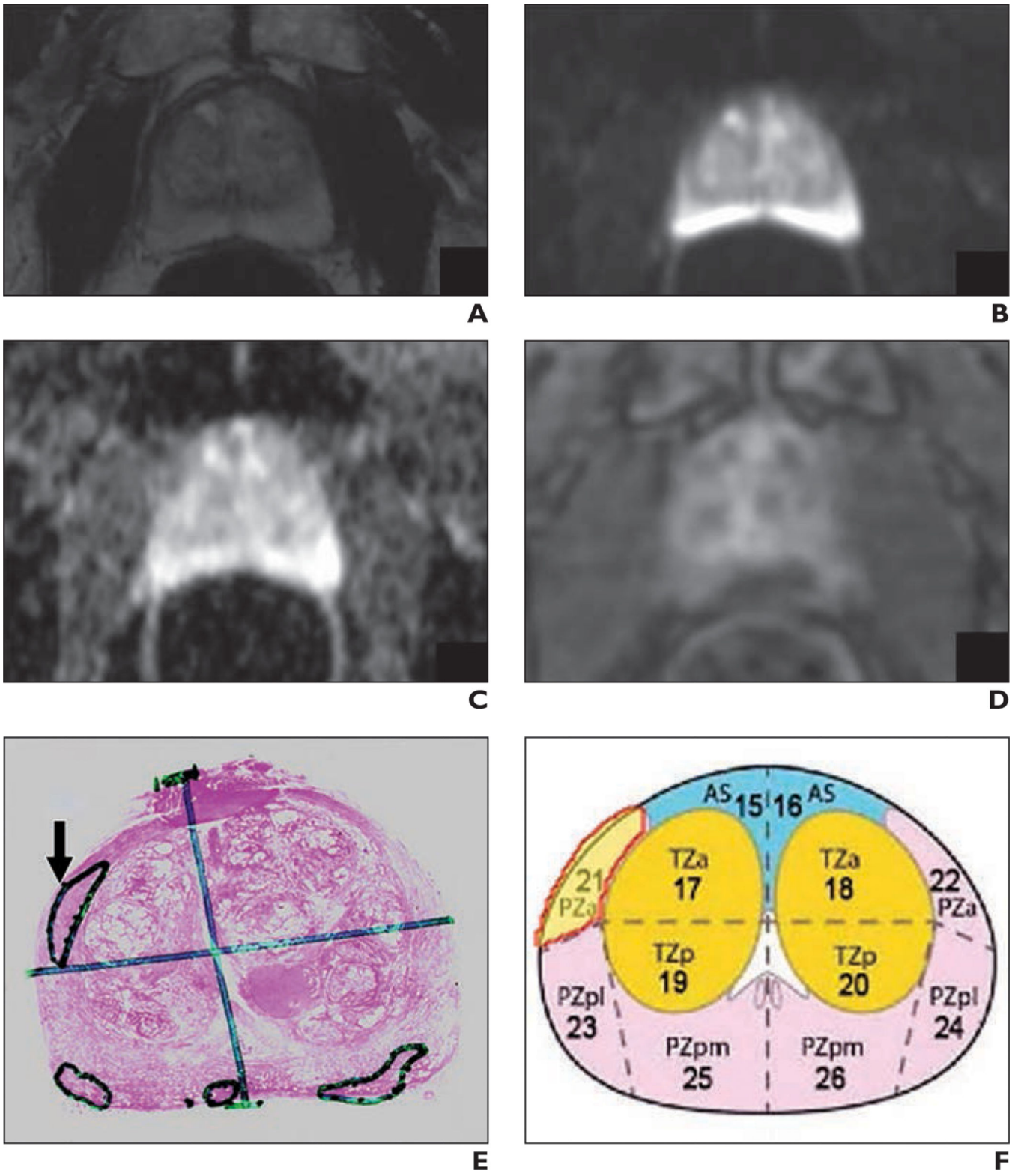

Fig. 5—.

Example of false-negative multiparametric MRI (mpMRI) finding for prostate cancer lesion when compared with whole-mount histopathology (WMHP) results is shown. Patient is 70-

year-old man who was referred for prostate mpMRI because of high serum prostate-specific antigen value (7.3 ng/mL).

A–D, Lesion is not visible on axial T2-weighted image (**A**), DW image (**B**), apparent diffusion coefficient map (**C**), and dynamic contrast-enhanced MR image (**D**).

Example of false-negative multiparametric MRI (mpMRI) finding for prostate cancer lesion when compared with whole-mount histopathology (WMHP) results is shown. Patient is 70-year-old man who was referred for prostate mpMRI because of high serum prostate-specific antigen value (7.3 ng/mL). **E,** Photomicrograph of thin section from whole-mount preparation of specimen obtained at radical prostatectomy shows 1.3-cm tumor (*arrow* and *upper outlined area*, Gleason score 3 + 3) in right anterior midlevel of prostate gland. Lower outlined areas show other foci of nontarget prostate cancer lesions. **F**, Drawing of prostate sector map based on Prostate Imaging Reporting and Data System version 2 (PIRADSv2). Numbers refer to sector number. WMHP results (**E**) show primary sector is sector 21 (*red outline*) at midgland level of prostate. AS = anterior fibromuscular stroma, PZ = peripheral zone, TZ = transition zone, a = anterior, p = posterior, pl = posterolateral, pm = posteromedial. (Adapted from American College of Radiology, PI-RADS: Prostate Imaging–Reporting and Data System 2015, version 2. Reston, VA: American College of Radiology, 2015 [29], with permission from the American College of Radiology)

TABLE 1:

Clinical and Pathologic Characteristics of Study Cohort

Characteristic	Value
No. of patients	415
Age (y), mean (range)	61.1 (38.0–80.0)
PSA level (ng/mL), mean (range)	8.1 (0.6–139.2)
Prostate volume (cm^3), mean (range)	41.4 (12.0–155.0)
PSA density ($ng/mL/cm^3$), mean (range)	0.20 (0.02–3.40)
Pathologic stage, no. (%) of patients	
T2	276 (66.5)
T3a	109 (26.3)
T3b	30 (7.2)
GS, no. (%) of PCa lesions (n = 863)	
≤ 6	408 (47.3)
3 + 4	298 (34.5)
4 + 3	97 (11.2)
8–10	60 (6.95)
Clinically significant PCa defined as GS ≥ 7, no. (%) of PCa lesions (n = 863)	455 (52.7)
Overall tumor diameter (cm), mean (range)	1.5 (0.05–5.0)
Base lesion (n = 76)	1.2 (0.1–3.5)
Midgland lesion (n = 441)	1.6 (0.05–5.0)
Apical lesion (n = 346)	1.3 (0.1–4.2)
Peripheral zone (n = 643)	1.4 (0.05–5.0)
Transition zone (n = 220)	1.6 (0.1–4.9)
Index tumor diameter (cm), mean (range)	2.1 (0.15–5.0)
Base lesion (n = 25)	2.1 (0.5–3.5)
Midgland lesion (n = 236)	2.2 (0.2–5.0)
Apical lesion (n = 154)	2.0 (0.15–4.2)
PZ (n = 311)	2.0 (0.15–5.0)
TZ (n = 104)	2.4 (0.2–4.9)

Note—PSA = prostate-specific antigen, GS = Gleason score, PCa = prostate cancer, PZ = peripheral zone, TZ = transition zone.

TABLE 2:

Characteristics of Prostate Cancer (PCa) Foci That Were Detected on Multiparametric MRI (mpMRI) and of PCa Foci That Were Missed on mpMRI

Characteristic	Total No. (%) of PCa Foci on mpMRI	No. (%) of Matching (TP) PCa Foci on mpMRI	*p*	No. (%) of Nonmatching (FN) PCa Foci on mpMRI
All PCa foci	863 (100) in 415 patients	419 (48.5) in 351 patients	< 0.0001[a,b]	444 (51.5) in 248 patients
Index tumors	415 (100)	322 (77.6)		93 (22.4)
Satellite (nonindex) tumors	448 (100)	97 (21.7)		351 (78.4)
Tumor location	863 (100)	419 (48.6)	0.04[a,c], 0.001[a,d], 0.97[e,f]	444 (51.5)
Base (76/863, 8.8%)	76 (100)	32 (42.1)		44 (57.9)
Midgland (441/863, 51.1%)	441 (100)	242 (54.9)		199 (45.1)
Apex (346/863, 40.1%)	346 (100)	145 (41.9)		201 (58.1)
Tumor zone	863 (100)		0.22[e,g]	
PZ (643/863, 74.5%)	643 (100)	324 (50.4)		319 (49.6)
TZ (220/863, 25.5%)	220 (100)	95 (43.2)		125 (56.8)
Index tumors Tumor location	415 (100)	322 (77.6)	0.02[a,c], 0.006[a,d], 0.45[e,f]	93 (22.4)
Base (25/415, 6.0%)	25 (100)	16 (64.0)		9 (36.0)
Midgland (236/415, 56.9%)	236 (100)	196 (83.1)		40 (17.0)
Apex (154/415, 37.1%)	154 (100)	110 (71.4)		44 (28.6)
Tumor zone	415 (100)		0.20[e,g]	
PZ (311/415, 74.9%)	311 (100)	246 (79.1)		65 (20.9)
TZ (104/415, 25.1%)	104 (100)	76 (73.1)		28 (26.9)

Note—TP = true-positive, FN = false-negative, PZ = peripheral zone, TZ = transition zone.

[a] Statistically significant *p* value.

[b] For comparison of index tumors and satellite tumors.

[c] For comparison of base lesions and midgland lesions.

[d] For comparison of midgland lesions and apex lesions.

[e] Not statistically significant *p* value.

[f] For comparison of base lesions and apex lesions.

[g] For comparison of PZ lesions and TZ lesions.

TABLE 3:

Sensitivity, Specificity, Positive Predictive Value (PPV), and Negative Predictive Value (NPV) of Multiparametric MRI for Overall Tumor Localization Based on 39-Segmentation Prostate Model From PI-RADS Version 2

Matching Approach, Lesion Group	Sensitivity (%)[a]	*p*	Specificity (%)[b]	PPV (%)[c]	NPV (%)[d]
Rigid, all tumors	28.5 (26.9–29.9)		96.3 (95.9–96.6)	68.4 (65.9–70.7)	82.7 (82.1–83.3)
Adjusted, all tumors	56.0 (54.0–58.0)		97.9 (97.6–98.1)	80.1 (78.0–82.0)	93.7 (93.2–94.1)
Rigid		< 0.001[e,f], < 0.001e,[g], 0.53[h,i]			
Base	19.0 (16.0–22.0)		97.0 (96.0–97.3)	42.0 (36.0–49.0)	90.0 (89.0–91.0)
Midgland	36.0 (34.0–38.0)		94.0 (93.0–95.0)	73.0 (70.0–76.0)	77.0 (77.0–78.0)
Apex	23.0 (21.0–26.0)		97.0 (96.0–97.0)	73.0 (69.0–77.0)	76.0 (75.0–77.0)
Adjusted		< 0.001[e,f], < 0.001[e,g], < 0.001[e,i]			
Base	35.8 (31.1–40.8)		97.6 (97.1–98.0)	56.0 (49.6–62.3)	94.7 (94.1–95.3)
Midgland	70.8 (67.7–73.7)		97.4 (96.8–97.8)	85.9 (83.1–88.3)	93.7 (92.9–94.4)
Apex	49.1 (45.5–52.7)		98.2 (97.7–98.5)	83.3 (79.5–86.5)	91.2 (90.3–92.0)
Rigid		< 0.001[e,j]			
PZ	30.3 (28.4–32.2)		93.9 (93.1–94.5)	71.5 (68.5–74.4)	72.6 (71.4–73.7)
TZ	24.5 (22.2–27.0)		97.2 (96.8–97.6)	61.6 (57.2–65.9)	87.6 (86.8–88.3)
Adjusted		0.04[e,j]			
PZ	58.9 (56.2–61.6)		96.9 (96.3–97.3)	82.3 (79.8–84.7)	90.4 (89.6–91.2)
TZ	51.2 (47.5–54.8)		98.3 (98.0–98.6)	75.5 (71.5–79.2)	95.3 (94.8–95.7)

Note—Values in parentheses are 95% CIs. PZ = peripheral zone, TZ = transitional zone, TP = = true-positive, FN = false-negative, TN = true-negative, FP = false-positive.

[a] $TP / (TP + FN)$.

[b] $TN / (TN + FP)$.

[c] $TP / (TP + FP)$.

[d] $TN / (TN + FN)$.

[e] Statistically significant *p* value.

[f] For comparison of base lesions and midgland lesions.

[g] For comparison of midgland lesions and apex lesions.

[h] Not statistically significant *p* value.

[i] For comparison of base lesions and apex lesions.

[j] For comparison of PZ lesions and TZ lesions.

TABLE 4:

Sensitivity, Specificity, Positive Predictive Value (PPV), and Negative Predictive Value (NPV) of Multiparametric MRI for Index Tumor Localization Based on 39-Segmentation Prostate Model From PI-RADS Version 2

Matching Approach, Lesion Group	Sensitivity (%)[a]	*p*	Specificity (%)[b]	PPV (%)[c]	NPV (%)[d]
Rigid, all tumors	34.3 (32.5–36.2)		96.3 (95.9–96.6)	64.7 (62.1–67.2)	88.1 (87.5–88.6)
Adjusted, all tumors	55.4 (53.1–57.8)		97.3 (97.0–97.6)	73.2 (70.7–75.5)	94.3 (93.9–94.7)
Rigid		< 0.001[e,f], < 0.001[e],g, 0.002[e],h			
Base	21.0 (17.3–25.3)		96.8 (96.2–97.3)	38.6 (32.4–45.2)	92.7 (91.9–93.4)
Midgland	43.7 (40.7–46.8)		94.2 (93.4–97.9)	70.1 (66.5–73.6)	84.3 (83.1–85.4)
Apex	29.0 (26.2–31.9)		96.4 (95.7–96.9)	69.4 (64.6–73.8)	82.8 (81.6–83.9)
Adjusted		< 0.001[e,f], < 0.001[e,g], < 0.001[e,h]			
Base	34.0 (28.9–39.5)		97.3 (96.8–97.7)	47.6 (41.1–54.3)	95.3 (94.7–95.9)
Midgland	71.3 (67.9–74.5)		96.3 (95.7–96.9)	79.2 (75.9–82.2)	94.5 (93.7–95.2)
Apex	47.8 (43.9–51.7)		97.6 (97.0–98.0)	73.1 (72.6–80.9)	91.7 (90.8–92.5)
Rigid		< 0.001[e,i]			
PZ	37.0 (34.6–39.5)		93.8 (93.1–94.5)	67.4 (64.1–70.6)	81.2 (80.1–82.3)
TZ	29.2 (26.4–32.2)		97.2 (96.7–97.5)	58.8 (54.2–63.3)	90.8 (90.2–91.5)
Adjusted		0.001[e,i]			
PZ	58.4 (55.4–61.3)		95.7 (95.1–96.2)	74.8 (71.7–77.7)	91.3 (90.4–92.0)
TZ	50.5 (46.6–54.3)		98.0 (97.7–98.3)	69.7 (65.4–73.8)	95.6 (95.1–96.1)

Note—Values in parentheses are 95% CIs. PZ = peripheral zone, TZ = transitional zone, TP = = true-positive, FN = false-negative, TN = true-negative, FP = false-positive.

[a] $TP / (TP + FN)$.

[b] $TN / (TN + FP)$.

[c] $TP / (TP + FP)$.

[d] $TN / (TN + FN)$.

[e] Statistically significant *p* value.

[f] For comparison of base lesions and midgland lesions.

[g] For comparison of midgland lesions and apex lesions.

[h] For comparison of base lesions and apex lesions.

[i] For comparison of PZ lesions and TZ lesions.